

Reconstructing a 51-year record of catchment scale dissolved load for the Haast/Awarua River in the Southern Alps, New Zealand

S.M. Mager^{a,*}, S.L. Horton^b

^a School of Geography, University of Otago, PO Box 56, Dunedin, New Zealand

^b School of Geography and the Environment, University of Oxford, UK

ARTICLE INFO

Keywords:

Mountain hydrology
Chemical weathering
Southern Alps
Dissolved load
Denudation

ABSTRACT

Mountains dominate global denudation fluxes of solutes to the oceans despite being only a modest portion of the Earth's surface. Determining the flux of material exhumed from mountains as dissolved load, however, requires careful measurement of ionic concentrations and discharge that may be hard to obtain. We reconstruct the dissolved load and total dissolved solids yield from pre-existing discharge measurements and 32-years on monthly water quality sampling in a headwater catchment in the Southern Alps/Ka Tiritiri o te Moana, New Zealand. The dissolved weathering yield of the Haast/Awarua River for 1971–2020 was $218 \pm 48 \text{ t km}^{-2} \text{ a}^{-1}$. The flux of dissolved material from the mountain catchment has a seasonal signal, with higher TDS concentrations during winter, but greater chemical weathering yields during summer. Hydrographic behaviour is an important control of weathering yields with 70 % of dissolved load being transported during event flow. Variations in chemical weathering yields are sensitive to changes in stream flow associated with broader climate oscillations, which will have a direct effect on estimations of chemical weathering rates since dissolved flux is strongly correlated to changes in stream flow.

1. Introduction

Headwater mountain catchments are areas of significant physical weathering (Milliman and Farnsworth, 2013), but the exhumation of lithic material, and/or the retreat of permanent snow and ice cover also reveals freshly exposed rock surfaces. These bare rock surfaces are key production zones for dissolved load due to the continual presence of water and carbonic acids from atmospheric CO_2 (Pope et al., 1995; Dixon and Thorn, 2005; Beylich and Laute, 2012b). The agency of water underpins both chemical and physical weathering processes so the maintenance of high chemical weathering rates is coupled to physical weathering processes (Gaillardet et al., 1999; Larsen et al., 2014). Chemical weathering rates are often inferred from riverine dissolved load as the sum of ionic mass flow-weighted and used as a proxy indicator of chemical denudation (Beylich and Laute, 2012a; Bouchez and Gaillardet, 2014). The exhumation and transportation of hillslope is derived from suspended sediment yields as a surrogate for physical weathering (e.g., Asselman, 1999; Piqué et al., 2017; Vercruysse et al., 2017) but the proportion of mass mobilised via dissolved load receives considerably less attention (Dixon and Thorn, 2005). Rather previous studies that have examined dissolved fluxes from mountain regions have

been more interested in determining chemical weathering fluxes for CO_2 drawdown rates (e.g. Gaillardet et al., 1999; Kump et al., 2000; Jacobson and Blum, 2003; Hilley and Porder, 2008; Liu et al., 2011; Donnini et al., 2016) rather than understanding its contribution to overall mass exhumation from hillslopes (Beylich and Laute, 2012a, 2012b; Mager et al., 2018).

The mean global yield of dissolved load for the 60 largest rivers in the world is $24 \text{ t km}^{-2} \text{ a}^{-1}$ but yields range from 6 to $338 \text{ t km}^{-2} \text{ a}^{-1}$ (Gaillardet et al., 1999) with the highest rates in regions with high rainfall, active tectonism, and lithologically soft terranes (Riebe et al., 2001; Millot et al., 2002; France-Lanord et al., 2003; Oliva et al., 2003). Neotectonic landscapes, like the Himalayas, have potent seismic disturbances that when combined with intense rainfall are ideal conditions to maximise denudation and stochastic hillslope failure (West et al., 2002; Gabet et al., 2010). Some of the globally highest chemical and physical weathering yields also occur on High Standing Islands (HSIs) like those in the Pacific where headwaters $> 1000 \text{ m asl}$ (Milliman and Syvitski, 1992) which are similarly subject to intense rainfall and seismic events. Collectively the rivers of Asia and HSIs of the Pacific contribute 35 % of the dissolved solids reaching the ocean (Milliman and Farnsworth, 2013).

* Corresponding author.

E-mail address: sarah.mager@otago.ac.nz (S.M. Mager).

<https://doi.org/10.1016/j.geomorph.2023.108807>

Received 2 September 2022; Received in revised form 5 June 2023; Accepted 26 June 2023

Available online 28 June 2023

0169-555X/© 2023 The Authors. Published by Elsevier B.V. This is an open access article under the CC BY-NC-ND license (<http://creativecommons.org/licenses/by-nc-nd/4.0/>).

The largest archipelago of the Pacific HSIs is Aotearoa New Zealand, which is situated along an active neotectonic plate boundary with the landmass oriented perpendicular to the westerly circulation belt. The Southern Alps/Kā Tiritiri o te Moana of Aotearoa New Zealand are the physiographic expression of a relatively young orogeny where high rainfall and suspended sediment rates (Hicks et al., 2011) provide ideal conditions for maximising physical and chemical weathering rates. Previous estimates of chemical weathering yields in the Southern Alps/Kā Tiritiri o te Moana range from 13 to 480 t km⁻² a⁻¹ (Lyons et al., 2005; Carey et al., 2006; Goldsmith et al., 2008; Moore et al., 2013; Mager et al., 2018). These data are either derived from small catchments (e.g., Mager et al., 2018), a small pool of exemplar catchments (e.g., Lyons et al., 2005; Carey et al., 2006), or regional-scale studies (e.g., Jacobson et al., 2003; Moore et al., 2013). Although useful, the previous studies of the chemical weathering flux of the Southern Alps/Kā Tiritiri o te Moana are mostly derived from one-off samples (e.g., Jacobson et al., 2003; Moore et al., 2013; Emberson et al., 2016) and do not account for seasonal variations in chemical weathering production, or, more importantly, variations in hydrological flow conditions that may substantially affect ionic concentration (the exceptions being Lyon et al., 2005 and Mager et al., 2018). As such, estimates of the dissolved load of the Southern Alps/Kā Tiritiri o te Moana are temporally constrained, usually to samples collected during the austral summer, and mostly do not consider the effect of event flow or seasonal changes in ionic production on dissolved flux.

A case study of a small headwater catchment on the eastern range front of the Southern Alps by Mager et al. (2018) showed that most of the dissolved load (77 %) was transported under base flow, and that the flux of dissolved material during summer was substantially higher than all other seasons. However, it is not known whether these interpretations are relevant for higher order catchments, or of flow conditions on the western range front, where mean annual rainfall frequently exceeds 6-m a year (Kerr et al., 2018). Furthermore, the multi-catchment studies (e.g., Jacobson et al., 2003; Moore et al., 2013) have not directly examined the hydrochemistry across hydrological years, nor considered the effects of decadal variability in sea surface temperatures and regional climate in

dissolved load estimates. Hydrochemical samples collected in summer, for example, may not be representative of year round conditions (Mager et al., 2018) because most of the mountain catchments of the Southern Alps/Kā Tiritiri o te Moana experience higher discharge during late spring and summer (Duncan and Woods, 2013). The higher incidence of snow melt and warmer temperatures are likely to be more conducive to chemical weathering, for example, than what may be observed year-round (Anderson et al., 1997; Gabet et al., 2010; Beylich and Laute, 2012a; Beylich and Laute, 2018), and consequently overestimate dissolved loads and chemical weathering yields.

The objective of this paper is to reconstruct a multi-decadal record of dissolved load flux that considers the effects of seasonal and multi-year variations in hydrochemistry. Specifically, we have developed a multi-year record of dissolved load for a near pristine mountain catchment in the western Southern Alps to assess: 1) temporal variations in dissolved load for seasonal, interannual, or decadal cycles; 2) the significance of event flow for transferral of dissolved load on a high-ordered catchment; and 3) the effect of time-scale for surrogate reconstructions of mean annual dissolved fluxes. To achieve this, we use a combination of flow records, long-term water quality monitoring data, and field data from the Haast/Awarua to reconstruct variations in dissolved load specific yields for a 51-year record (1971–2021).

2. Materials and methods

2.1. Study location and physiography

Haast/Awarua is a steep, six-order alpine catchment (Fig. 1) situated on the western range front of the Southern Alps/Kā Tiritiri o te Moana in Aotearoa New Zealand. The Haast/Awarua drains 1356 km² of unmodified cool temperate rainforest with tussock grasslands and herbfields above the tree line. The climate is pluvial and maritime (Köppen Classification Cfb) with a mean annual normal air temperature (1991–2020) of 8.3 °C (measured at Haast township 43.8600°S, 169.0065°E at 1 m asl), with seasonal mean temperatures of 14.5 °C (summer) and 8.2 °C (winter). Permanent snow and ice covers 4 % of the

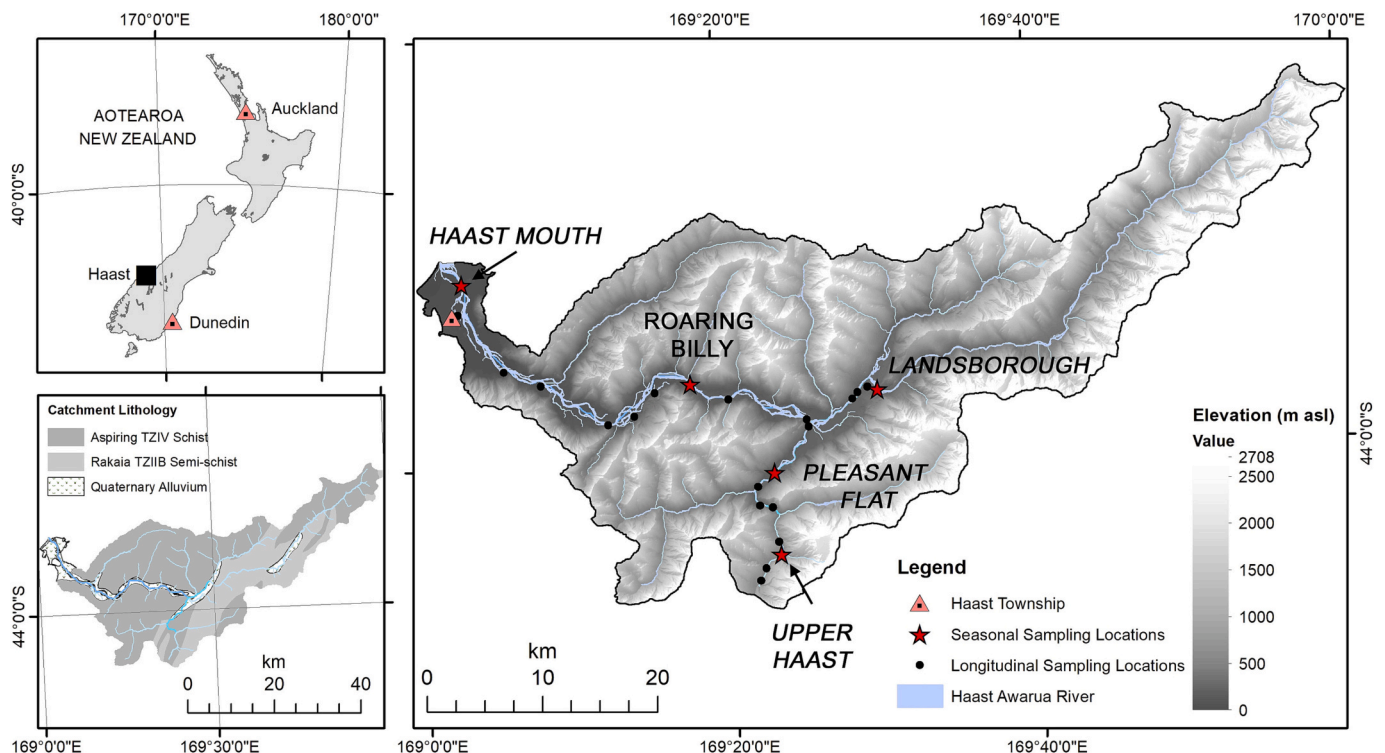


Fig. 1. Location of the Haast/Awarua River in southwest New Zealand.

catchment, with numerous small alpine glaciers. The Brewster Glacier (3 km²) is the largest glacier in the headwaters of its eponymous tributary, but its main tributary (the 'Landsborough') contains the remaining 90 % of the snow, ice fields and glaciers. The indigenous name *Awarua* ("two rivers") is synonymous with the catchment morphology; two main tributary rivers ('Haast' and 'Landsborough') that flow north, and southwest respectively, to converge 42 km from the river mouth. Exposed bedrock and scree deposits occur throughout the catchment and the main river network sits within a broad alluvium-filled multi-threaded river network of gravels (Fig. 2), with boulder cascades in the upper reaches (Fig. 2b). Gravel and bare rock comprise 12.6 % of the catchment area. Bedrock lithology comprises Aspiring Association TZIV Rakaia Terrane schist and Rakaia terrane semi-schist (TZIIIB), the latter semi-schist lithology is principally within the Landsborough Valley (Rattenbury et al., 2010). Stream flow and precipitation are measured at Roaring Billy (Fig. 1) with a median annual discharge of 124 m³ s⁻¹ and mean annual precipitation of 5270 mm a⁻¹. Area-weighted catchment precipitation is considerably higher at 7617 mm a⁻¹ due to orographic uplift on the stoss face of the Alps as estimated from a National gridded thin-spline interpolation model (see: Tait et al., 2006). Suspended sediment yield at Roaring Billy is 4072 t km⁻² a⁻¹ derived from 45 samples rated to discharge (Hicks et al., 2011).

2.2. Data collection

The Haast/Awarua is one of 77 catchments within the National River Water Quality network (NRWQN) and a benchmark water quality site where streamflow has been continuously recorded at Roaring Billy (43.942°S 169.298°E) since May 1970 (stage-discharge rated with discharge recorded at 15-minute intervals) and maintained by NIWA Taihoro Nukurangi (NIWA, 2019). Monthly in situ water quality observations and sample collection began in May 1989 ($n = 388$ to December 2021). For the first year of the NRWQN (1989–1990) major cations and anions were collected (Na⁺, K⁺, Ca²⁺, Mg²⁺ Alkalinity, Cl⁻, and SO₄²⁻) and quantified using atomic absorption spectroscopy, titration, and colorimetric analysis ($n = 12$).

Discrete grab samples were collected at three locations (Table 1)

along the main stem of the Haast/Awarua River, and occasionally from the Landsborough River (Table 2). Specific electrical conductance (in $\mu\text{S cm}^{-1}$) was measured at each sample location using an YSI Pro Plus probe, with an instrumental precision of $\pm 0.5\%$. An ISCO water sampler collected hourly 500 mL samples over three events ($n = 95$). Event bulk rain samples were collected adjacent to the river channel into a HDPE funnel and 2 L container near the Roaring Billy tipping rain bucket, and in the Upper Haast tributary.

Major and minor ion concentrations were measured using a Dionex 3000 ion chromatograph (F⁻, Cl⁻, Br⁻, NO₃⁻, SO₄²⁻) and a Spectro-Blue inductively coupled plasma optical emission spectrometer (Na⁺, K⁺, Ca²⁺, Mg²⁺, Total Si, Al³⁺, Total Fe, Sr²⁺, Zn²⁺). Analytical precision was $<0.1 \text{ mg L}^{-1}$ for all major analytes and $<0.001 \text{ mg L}^{-1}$ for minor analytes and summed to ensure a charge balance error $<5\%$. The $\delta^{13}\text{C}_{\text{DIC}}$ were collected directly from the river into 100 mL borosilicate bottles with no headspace, preserved with HgCl₂, sealed until measurement with a Thermo Delta Plus Advantage IRMS. Dissolved organic carbon (DOC), particulate organic carbon (POC), dissolved inorganic carbon (DIC) and $\delta^{13}\text{C}_{\text{DIC}}$ samples were collected from the main stem and significant tributaries ($n = 88$) and reported relative to the international standard vPDB (Vienna Pee Dee Belemnite) DOC was analysed using a Shimadzu Total Carbon Analyser (detection limit 0.5 mg C L⁻¹ and precision of 0.1 mg C L⁻¹); POC was determined by loss on ignition assuming a van Bemmelen factor of 2 (see: Bright et al., 2020a); and DIC was determined by titration following standard methods. Chemical weathering fluxes were estimated using end member mixing based on $\delta^{13}\text{C}_{\text{DIC}}$ (see: Phillips and Gregg, 2001).

A 1 kg sample of bed sand was collected at the waters edge from four locations: Upper Haast, Roaring Billy, Haast Mouth, and Landsborough. Sediment samples were dried at 105 °C for 72 h, sieved at 0.5 phi intervals and the medium-sized sand fraction (+1.5 phi size, 354 μm) material retained for geochemical analysis. Suspended sediment (SS) was collected during event flow at Roaring and the Landsborough, left to settle then separated from the water, dried at 35 °C for 72 h, and retained for geochemical analysis (see: Bright et al., 2020b for method). Bed sand and suspended sediment samples were analysed using portable X-ray fluorescence with a Delta Premium DP-6000 portable XRF

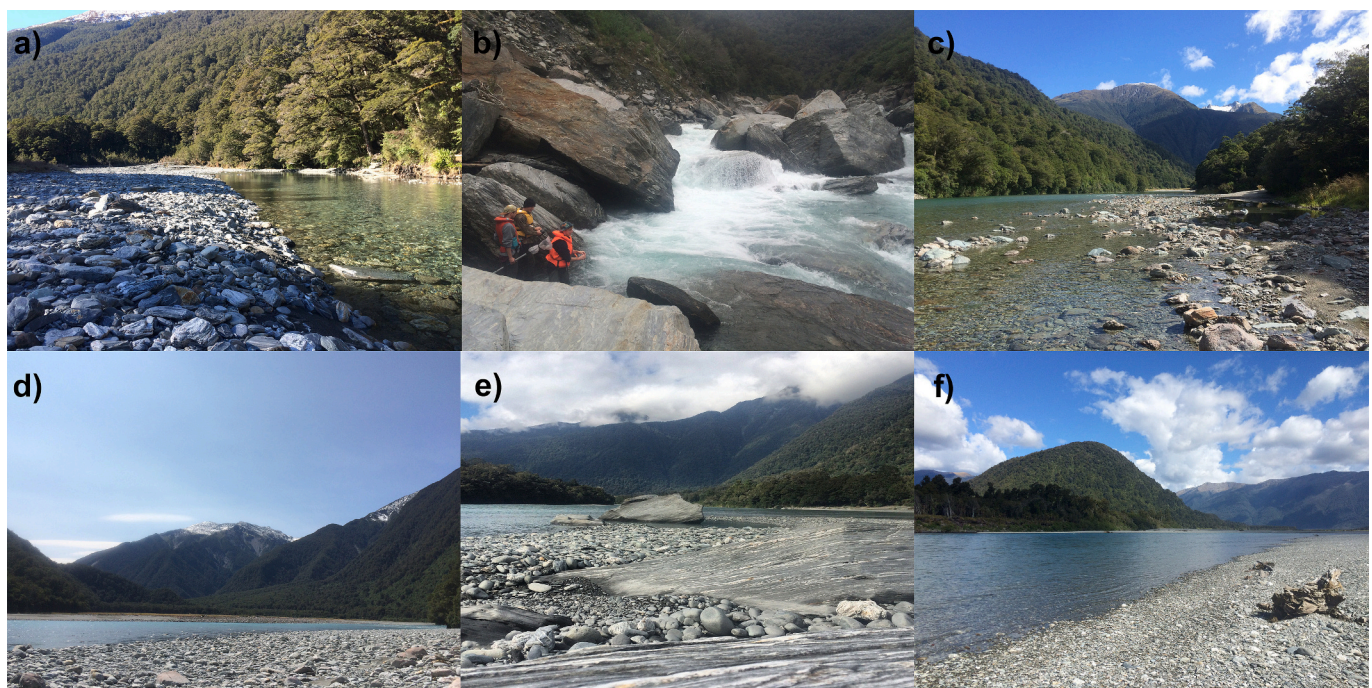


Fig. 2. Haast/Awarua River in South Westland, New Zealand at a) Upper Haast tributary near Fantail Falls, b) Gates of Haast, c) Pleasant Flat above Landsborough confluence, d) Landsborough at Strutt Bluff, e) Roaring Billy Gauging Site, and f) downstream of Haast Township.

Table 1
Sampling locations used in Haast Awarua catchment.

Sampling location	Latitude (°S)	Longitude (°E)	Sampling elevation (m asl)	Mean elevation (m asl)	Area (km ²)	Est. mean discharge (m ³ s ⁻¹)	Est. runoff (mm a ⁻¹)
Upper Haast	44.076	169.388	540	1142	30	5	5260
Haast at Pleasant Flat	44.013	169.383	80		255	47	5816
Landsborough	43.950	169.500	100	1140	354	65	5794
Roaring Billy	43.936	169.288	59	1055	1063	191	5670
Haast at Mouth	43.856	169.054	3	950	1356	213	4957

Table 2
Collection dates for water samples collected in Haast/Awarua catchment.

Sampling type	Location (s)	Analysis	Sampling resolution	No. samples
NRWQN sampling (1989–1990)	Roaring Billy	Major and minor analytes, N, P, EC, DIC, temperature, turbidity, visual clarity	Monthly	12
NRWQN Benchmark sampling (1989–2021)	Roaring Billy	N, P, EC, temperature, turbidity, visual clarity	Monthly	388
Seasonal sampling (2012–2017)	Upper Haast Roaring Billy Haast Mouth	Major and minor analytes, N, P, EC, DIC, temperature, turbidity, SS, POM, DOC, $\delta^{13}\text{C}_{\text{DIC}}$	Quasi-quarterly 28-Jan-12, 26-Oct-12, 12-Dec-12, 10-Apr-13, 11-Aug-13, 8-Nov-13, 1-Mar-14, 22-May-14, 27-Aug-14 ^c , 5-Nov-14 ^c , 6-Feb-15 ^a , 4-Sep-15, 12-May-17	39
Longitudinal sampling (2015–2017)	19 locations along main stem	Base cations, silica, POM/POC, DOC, DIC, $\delta^{13}\text{C}_{\text{DIC}}$, in situ EC	Quasi-quarterly 6-Feb-15, 26-Mar-16 ^a , 3-Jun-16, 2-Sep-16, 5-Nov-16, 6-Feb-17, 27-Mar-17	133 88 ($\delta^{13}\text{C}$)
Event sampling (2019–2020)	Roaring Billy	Major and minor analytes, DIC, EC, turbidity, SS, POM	Summer event flows 19/20-Jan-19 18/20-Feb-19 ^{a,b} 11/13-Jan-20 4/5-Feb-20	155

^a Also collected in the Landsborough.^b Samples collected in the Upper Haast at Pleasant Flat.^c Seasonal sampling rounds that included $\delta^{13}\text{C}_{\text{DIC}}$.

(Olympus) in *geochem* mode. The geochemistry is reported in parts-per million notation, which was normalised to a weight per cent (wt%) for the major oxides. Bed sand mineralogy was determined using single-crystal X-ray diffraction (XRD) with an individual particle diameter of <80 μm using a PANalytical X'Pert PRO MPD diffractometer at the University of Otago.

2.3. Data analysis

River samples were adjusted to account for solute input from atmospheric deposition by removing the component of ionic flux contributed by precipitation. The Haast/Awarua riverine chloride has a single source

origin (that is, rainfall) as there are no significant evaporites or hot springs in the catchment. The proportion of chloride relative to other ions was used to determine the precipitation input (see: Moore et al. (2013)). The ionic load of precipitation for the Haast/Awarua is very low (<2 $\mu\text{S cm}^{-1}$) despite its close proximity to the ocean and contributes <7 % to the total riverine dissolved load. The resultant precipitation-adjusted concentrations (denoted with *) for the major and minor ions were summed to calculate the total dissolved solids (TDS*) within the river water samples. The TDS* is assumed to be equivalent to the load of dissolved material attributable to chemical weathering. Linear least squares regression analysis was used to convert the catchment-specific rating of TDS* to in situ specific electrical conductance (EC), because EC is a measure of the ionic strength of water and directly proportional to the sum of dissolved ions (Hubert and Woldersdorfer, 2015). Thus, measurements of EC were used to estimate the dissolved load over time series when there were no direct measurements of TDS. Monthly dissolved load from 1989 to 2021 was calculated by multiplying the instantaneous discharge associated with in situ EC measurements by assuming that the total dissolved solids (TDS*, in g m^{-3}) ratio of Specific EC to TDS* had remained constant over time (and validated from major cation and anion chemistry collected in 1989 and samples collected between 2012 and 2017). A 51-year record of dissolved load (as TDS*) was reconstructed at a daily and monthly time step by rating Specific EC (in $\mu\text{S cm}^{-1}$) to flow records ($\text{m}^3 \text{s}^{-1}$) using in situ measurements collected from 1989 to 2021.

3. Results and discussion

3.1. Hydrochemistry, geochemistry and carbon uptake

The hydrochemistry of Haast/Awarua River is a Ca-HCO_3 dominant water type, typical of rivers draining the schistose lithology of the main divide of the Southern Alps (Table 3). Solute concentrations were low with specific electrical conductance averaging 75 $\mu\text{S cm}^{-1}$ under base flow conditions in the Upper Haast and Roaring Billy sampling locations, and 95 $\mu\text{S cm}^{-1}$ for the Landsborough tributary. During event flow there was a dilution effect so that median EC measured 24 $\mu\text{S cm}^{-1}$, with a minimum of 15–20 $\mu\text{S cm}^{-1}$. Total dissolved solids were low: median total dissolved solids (TDS) were 40.9 mg L^{-1} ($n = 94$). Precipitation had a very low ionic concentration (Table 3) but varied between sampling locations, within and between events. For example, higher Cl^- was observed at the coast with ionic depletion further inland and systematic rainout of ions over a rain event. The rainout of ions over events, in particular, warrants ensuring that rainfall collection is from the entire rain event (i.e., as ‘bulk’ rainfall).

Comparison between the hydrochemistry collected in 1989–1990 and samples from 2012 to 2017 showed that the major ionic composition is static (Fig. 3), and that no significant shifts in hydrochemistry have occurred over the last 30 years. Ionic plots (in units of $\mu\text{eq L}^{-1}$) showed strong relationships (Fig. 4) between the sum of calcium and magnesium ($\text{Ca}^{2+} + \text{Mg}^{2+}$), the sum of bicarbonate and sulfate ($\text{HCO}_3^- + \text{SO}_4^{2-}$), and with total base cations ($r^2 = 0.99$). As expected for the schist/semi-schist lithology the ionic composition is principally via carbonate chemical weathering (Fig. 4). Mechanical exposure of fresh rock surfaces, particularly hydrothermally-altered veins within the schistose

Table 3

Hydrochemistry composition of surface water and precipitation in the Haast/Awarua catchment. All concentrations are in units of milligrams per litre (mg L^{-1}), except Specific Electrical Conductance (EC, in $\mu\text{S cm}^{-1}$). ND indicates no data and the dash indicates concentrations below method detection limits.

	Na^+	K^+	Ca^{2+}	Mg^{2+}	Si^{T}	Cl^-	SO_4^{2-}	NO_3^-	HCO_3^-	Al^{2+}	Fe^{T}	Sr^{2+}	EC
<i>Upper Haast (450 m asl) (n = 20)</i>													
Mean	0.88	0.22	6.3	0.40	1.3	0.57	3.1	0.01	17.8	0.009	0.008	0.026	75.0
Median	0.91	0.21	6.0	0.38	1.4	0.59	3.1	0.02	17.5	0.006	0.004	0.026	75.0
<i>Roaring Billy 1989–1990^a (80 m asl) (n = 12)</i>													
Mean	1.28	0.83	12.3	0.69	ND	0.72	4.3	0.04	30.3	ND	ND	ND	76.5
Median	1.20	0.83	12.6	0.72	ND	0.75	4.5	0.04	31.8	ND	ND	ND	77.5
<i>Roaring Billy (80 m asl) (n = 20)</i>													
Mean	1.13	0.75	8.5	0.64	1.5	0.80	4.7	0.03	27.1	0.012	0.013	0.061	72.6
Median	1.18	0.73	9.3	0.64	1.6	0.81	4.3	0.02	27.9	0.011	0.010	0.062	74.4
<i>Landsborough (120 m asl) (n = 3)</i>													
Mean	1.16	0.35	7.9	0.87	1.5	0.45	7.4	0.03	24.8	0.006	0.005	0.072	94.6
<i>Event flow at Roaring Billy Feb-19 (n = 55)</i>													
Mean	0.82	0.66	8.3	0.49	ND	0.56	3.4	0.02	27.5	0.019	0.032	0.052	26.0
Median	0.79	0.67	8.0	0.47	ND	0.53	3.3	0.02	26.7	0.015	0.007	0.053	23.9
<i>Bulk rain collected at Upper Haast/Awarua Valley (560 m asl)</i>													
19/01/19	0.05	0.01	0.09	0.01	–	0.10	0.17	–	ND	–	–	–	<1
20/01/19	0.70	0.06	0.08	0.09	–	1.22	0.26	0.01	ND	–	–	–	2.2
21/02/19	0.11	0.02	0.03	0.02	–	0.18	0.20	0.05	ND	–	–	–	<1
<i>Bulk rain collected at Roaring Billy Gauging Station (80 m asl)</i>													
19/01/19	0.08	0.01	0.05	0.01	–	0.14	0.20	0.04	ND	–	–	–	<1
20/01/19	0.02	0.01	0.03	0.01	–	0.05	0.13	–	ND	–	–	–	<1
18–19/02/19	0.31	0.02	0.07	0.05	–	0.57	0.23	0.03	ND	–	–	–	<2
19–20/02/19	0.50	0.03	0.05	0.06	–	0.86	0.29	0.04	ND	0.002	–	–	<2
<i>Bulk rain collected in Landsborough Valley (100 m asl)</i>													
18–20/02/19	0.15	0.02	0.05	0.02	–	0.25	0.19	0.06	ND	–	–	–	<1
<i>Precipitation-adjusted concentration (all location, excluding event flows, n = 94)</i>													
Mean	0.71	0.43	8.21	0.51	1.10	–	3.55	0.02	23.81	0.012	0.013	0.049	64.0
Median	0.68	0.38	7.63	0.54	1.18	–	3.55	0.02	23.48	0.011	0.007	0.049	63.2

^a Geochemical data extracted from the NRWQN database maintained by NIWA.

lithology, are also conducive to sulfide weathering (e.g., Campbell et al., 2002; Anderson, 2005), which likely contributes sulfur to the solute flux, particularly in the semi-schist terranes of the Landsborough, which has substantially higher sulfate concentrations (mean: 7.4 g m^{-3}), compared to the eponymous Haast tributary (mean: 4.5 g m^{-3}).

Hydrochemical analysis showed that calcium contributed ~83 % of the total cation concentration (in $\mu\text{eq L}^{-1}$), however, it is a relatively minor constituent of particulate geochemistry (e.g., <2 wt% of bed sands and suspended load) and 2–6 wt% of the basement lithology (Roser and Cooper, 1990) (Table 4). Silicates in the form of quartz and phyllosilicates (muscovite, chlorite-serpentine, and vermiculite) were detected by XRD in bed sand from Roaring Billy, as well the feldspathic mineral, albite. The particulate geochemistry is dominated by silica (SiO_2), aluminium oxide (Al_2O_3), and iron oxides (reported as total iron oxides, FeOT). Vermiculite was also detected by XRD and is likely a by-product of the breakdown of muscovite mica through silicate weathering. Calcite and albite are potential sources of rock-derived calcium carbonate, although at Pleasant Flat where the Landsborough and Haast converge there is a suite of carbonate-rich metamorphic dykes (Cooper and Paterson, 2008). These carbonatite-dykes comprise of <1 % of the total rock mass, but may be an important local source of calcium carbonate, as well as being relatively enriched in trace metals Ba, Th, Sr, Zr and Y (Cooper and Paterson, 2008). The relatively high concentration of Ca^{2+} within the dissolved load and low concentration of CaO in the particulate load of the Haast/Awarua shows that calcium is

preferentially exhumed from the catchment in dissolved load rather than as particulate load.

Silicate weathering was a small component of the dissolved load in the Haast/Awarua. Silica (reported as total dissolved silicon, Si^{T}) was equivalent to 2.8 % of the total dissolved load (with a mean concentration of 1.3 g m^{-3}), but silica (reported as SiO_2) was the main constituent of bed sand (wt%) and suspended particulate material (>63 wt %). Thus, the flux of silica through the Haast/Awarua is particulate, as either suspended or bedload and dissolved silica is only a small contributor to overall chemical weathering fluxes. Silica is a non-conducting material within water samples and is not detected from in situ measurements of electrical conductance (Hubert and Woldersdorfer, 2015). However, the concentration of dissolved silica (Si^{T}) is rateable to specific EC in the Haast/Awarua (Fig. 4), since it is governed by weathering processes that produce the other main dissolved load constituents. Thus, the total dissolved solids (which includes Si^{T}) in units of mass concentration can be predicted from in situ Specific EC, which has a very strong linear relationship (Fig. 4c). Thus, specific EC can be used as a surrogate of TDS, and when calibrated to local river and rainfall ionic composition these data can be used to produce a rating equation for TDS* (Fig. 4d).

Dissolved inorganic carbon (DIC) was the largest dissolved carbon flux through the Haast/Awarua with a median concentration of 5.1 mg L^{-1} , equivalent to $25.4 \text{ t C km}^{-2} \text{ a}^{-1}$, relative to dissolved organic carbon concentrations of 1.7 mg C L^{-1} , and equivalent to $8.5 \text{ t C km}^{-2} \text{ a}^{-1}$.

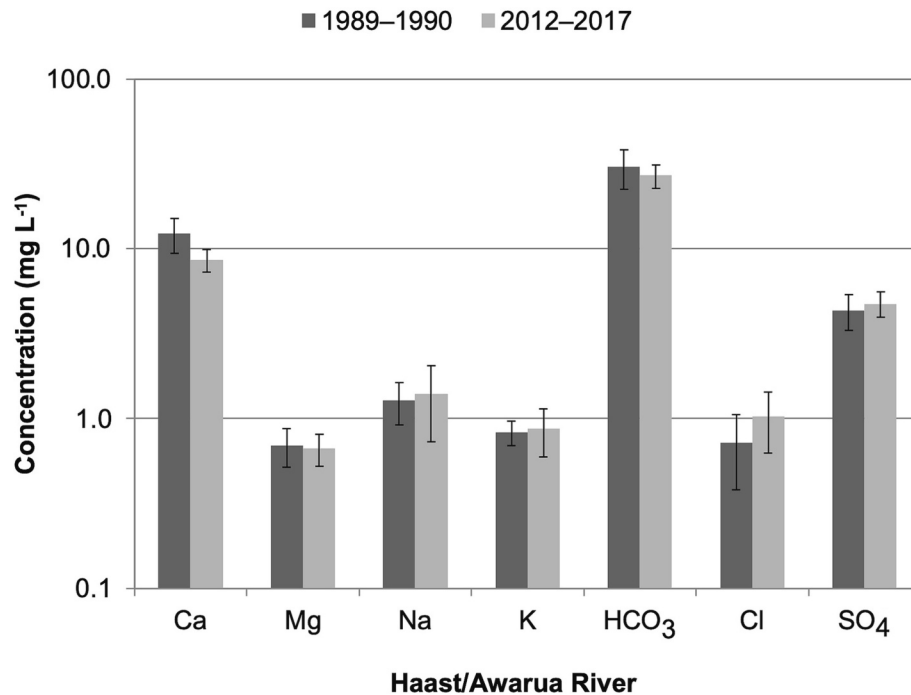


Fig. 3. Major ionic composition of river samples collected from Roaring Billy gauging site on the Haast/Awarua for 12 samples collected from 1989 to 1990 by NIWA, and 16 samples collected from 2012 to 2017. Error bars are the standard deviation from the mean for each data set.

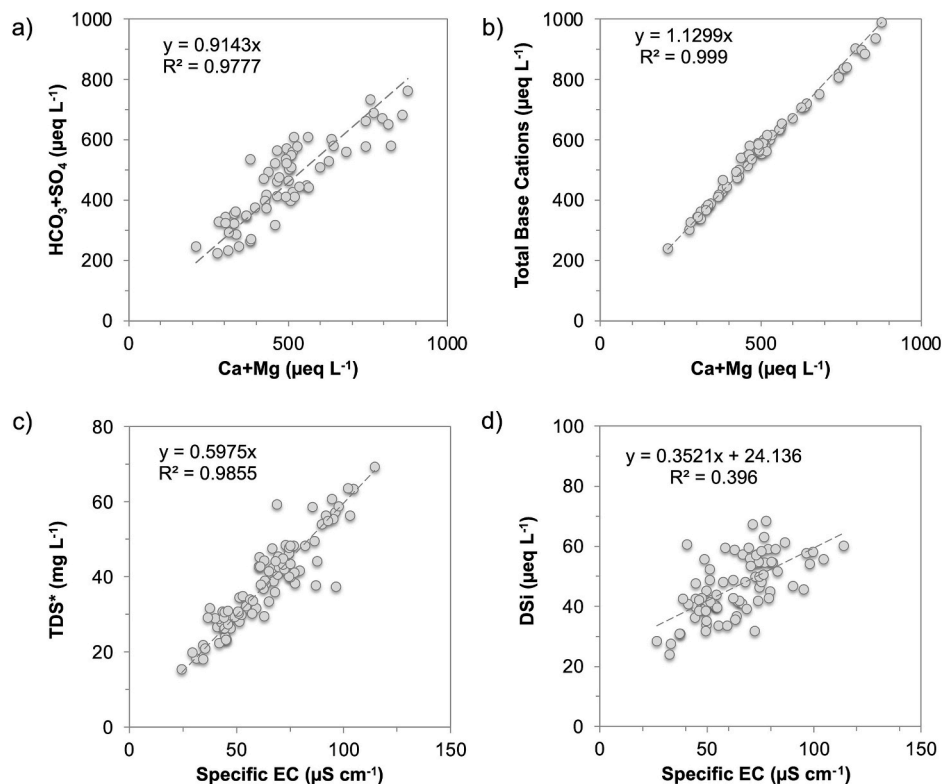


Fig. 4. Hydrochemical bivariate plots for chemical weathering relationships, and relationships between specific electrical conductance and precipitation-adjusted total dissolved solids (TDS*) and dissolved silica (DSi).

Particulate organic matter (POM) was $\leq 2\%$ of the particulate load during event flow (Bright et al., 2020b). POC is approximately half of POM so POC as a proportion of annual suspended sediment would yield an additional $40.7 \text{ t C km}^{-2} \text{ a}^{-1}$ of organic carbon discharged to the coast. Thus, although the main type of chemical weathering is via

carbonate weathering, the principle flux of carbon from the catchment is organic ($\cong 49 \text{ t C km}^{-2} \text{ a}^{-1}$ or $66,580 \text{ t C a}^{-1}$).

Median $\delta^{13}\text{C}_{\text{DIC}}$ near the river mouth of the Haast/Awarua was -7.9‰ (Table 5) and is depleted relative to atmospherically-derived $\text{CO}_{2(\text{aq})}$ of $\delta^{13}\text{C} -1\text{‰}$ (Mook, 2006). The riverine $\delta^{13}\text{C}_{\text{DIC}}$ in the Haast/Awarua

Table 4

Mean geochemistry of particulate load at Haast/Awarua River determined using portable X-ray fluorescence.

	Bed sand			Suspended sediment		Lithology	
	Roaring Billy	Upper Haast	Lands-borough	Lands-borough	Roaring Billy	Aspiring Terrane ^a	Haast Schist ^a
<i>Major oxides (wt%)</i>							
SiO ₂	71.16	67.83	67.79	63.22	66.22	71.09	66.63
Al ₂ O ₃	13.65	15.19	16.04	17.88	16.48	13.32	14.24
FeOT	4.94	6.65	5.22	6.55	5.99	3.21	4.07
CaO	1.27	1.32	1.01	1.01	1.58	2.24	6.11
K ₂ O	2.70	2.96	3.81	5.20	3.56	1.76	2.50
TiO ₂	0.69	0.44	0.37	0.41	0.47	0.44	0.65
MnO	0.08	0.10	0.12	0.15	0.09	0.05	1.41
P ₂ O ₅	0.00	0.00	0.00	0.00	0.00	0.06	0.13
MgO						1.26	1.41
Na ₂ O						4.34	2.29
<i>Trace elements (ppm)</i>							
Ba	521	622	796	848	688–814	441	640
Cr	–	–	51	74	29–55	21	31
Nb	12	11	15	15	14	8	8
Ni	–	–	117	–	–	8	12
Pb	22	18	15	41	24–34	18	24
Rb	94	109	150	237	139–210	69	97
Sr	309	301	311	354	348	192	412
Ta	48	46	50	86	55–82	ND	ND
Th	14	8	14	18	13	7	9
Y	21	25	23	26	26–31	12	20
Zn	84	106	93	157	121	52	59
Zr	195	167	191	194	197–253	117	175

^a XRF data for Aspiring lithological association psammites and Haast schist at Big Bluff at 8 m depth in Haast catchment as reported in Roser and Cooper (1990).**Table 5**Carbon concentrations in the Haast Awarua River from samples collected from longitudinal river sampling ($n = 160$ except $\delta^{13}\text{C}$ where $n = 88$). BDL indicates below detection limit for POC method (0.1 mg C L^{-1}). Numbers in brackets are the median value.

Location	Organic carbon		Inorganic carbon			
	POC (mg C L^{-1})	DOC (mg C L^{-1})	DIC (mg C L^{-1})	$\delta^{13}\text{C}_{\text{VPDB}}$ (‰)	CO_2 (atm) (t C km^{-2} a^{-1})	CO_2 (atm) (10^5 mol km^{-2} a^{-1})
Upper Haast	BDL	0.7 to 4.3 (1.8)	1.5 to 4.9 (3.7)	−5.8 to −7.9 (−6.6)	14.8	12.3
Roaring Billy	BDL to 0.15	1.3 to 4.4 (1.8)	2.8 to 7.3 (4.3)	−7.4 to −9.8 (−8.1)	17.4	14.5
River Mouth	BDL to 1.2 (0.37)	1.1 to 4.8 (1.7)	4.3 to 6.8 (5.1)	−7.1 to −8.8 (−7.9)	17.7	14.7

is much closer to rock-derived carbonate, which locally has carbonatite deposits of $\delta^{13}\text{C}$ −5.5 to −7.1 ‰ (Blattner and Cooper, 1974). Given that aqueous $\delta^{13}\text{C}_{\text{DIC}}$ of −7.9 ‰ is less than the lithological-source range and that rock weathering of carbonate-minerals also consumes CO_2 , there must be contributions of soil-derived CO_2 (Finlay, 2003), the latter of which has an aqueous fractionation equivalent of $\delta^{13}\text{C}$ −24 ‰ (Cerling et al., 1991) for indigenous C_3 -derived plant material (see: Rounick et al., 1982, Stewart and Metherell, 1999). To maintain a riverine $\delta^{13}\text{C}_{\text{DIC}}$ of −7.9 ‰ carbonate chemical weathering in the Haast/Awarua is likely augmented by carbonic acid derived from soil microbial respiration and soil water leachate from forest soils. Based on end member mixing (see: Phillips and Gregg, 2001), the mixing ratio of CO_2 (soil) relative to CO_2 (atm) was between 0.24 (Upper Haast) and 0.30 (discharged at mouth). These data suggest that most CO_2 (aq) is sourced from atmospheric equilibration and that CO_2 (atm) effluxed from the Haast catchment at the coast is ≈ 23.7 % of the total carbon flux equivalent being to $17.7 \text{ t C km}^{-2} \text{ a}^{-1}$. The CO_2 (atm) uptake attributable to chemical weathering is equivalent to $14.7 \times 10^5 \text{ mol CO}_2 \text{ km}^{-2} \text{ a}^{-1}$

and of similar magnitude as reported for the Himalayas, HSI's, and India (Hren et al., 2007; Goldsmith et al., 2010; Nisha et al., 2021), but twice as large as uptakes rates reported for Europe and Brazil (Donnini et al., 2016; Machado et al., 2021).

3.2. Seasonal variations in dissolved solid flux

The 32-year record of monthly river sampling from the NRWQN shows that there is a small difference in dissolved solid concentrations (and flux) between seasons. Higher dissolved solid concentrations occur in winter (mean TDS* of 49 mg L^{-1}) compared to summer (mean TDS* of 42 mg L^{-1}) (Table 6). These differences likely occur due to decreases in runoff that occur during winter when snow storage is greatest, so there is a lower dilution effect as river flows tend to be lower during winter. Accounting for variations in flow, the dissolved solid yield is 42 % lower in winter compared to summer (e.g., 153 cf. $267 \text{ t km}^{-2} \text{ a}^{-1}$) and underscores the potential for over-estimation of chemical weathering rates from summer-only derived sampling. During summer glacially augmented weathering is most active, and is likely the dominant source of solutes through the exhumation of fresh mineral surfaces from glacial abrasion (Anderson, 2005; Gabet et al., 2010). In winter, however, solute production is reduced due to increased snow and ice storage and a substantial decline in glacial melt and runoff, so that runoff and solute load are sustained from non-glacial chemical weathering processes (e.g., Anderson et al., 1997).

Table 6Seasonal estimates of total dissolved solids concentration (TDS*), flux (TDS_f*) and yield (DSY) for precipitation-adjusted ionic flux in the Haast/Awarua catchment for monthly samples collected between 1989 and 2021 ($n = 388$).

	TDS* (mg L^{-1})	TDS _f * (t day^{-1})	DSY (t $\text{km}^{-2} \text{ a}^{-1}$)
Summer	42.0	779.1	267.5
Autumn	46.1	581.2	199.6
Winter	49.0	446.0	153.2
Spring	43.8	637.1	218.7
All Data	45.3	608.8	209.0

3.3. Event-flow patterns in chemical weathering fluxes

Analysis of the response of Specific EC to event flow discharge shows that dissolved load is strongly related to discharge in the Haast/Awarua River. Analysis of Specific EC (and its surrogate TDS*) showed no evidence of hysteretic responses in dissolved ions during events and that the relationship between Specific EC and discharge was consistent between events (Fig. 5a). These data validated the approach that discharge could be used as a surrogate for Specific EC and TDS* for both base flow and storm flow conditions.

High quality hourly flow data (Q) from Roaring Billy was used for the period 2000–2021 to reconstruct an hourly resolution estimate of the chemical weathering flux using the EC–Discharge rating curve to ascertain the significance of event flow to annual estimates of dissolved load. Data were summed to calendar years as a mean dissolved solids flux observed at or below median flow i.e., base flow as derived from the flow records (when $Q < 120 \text{ m}^3 \text{ s}^{-1}$), or during event flow (when $Q > 120 \text{ m}^3 \text{ s}^{-1}$) (Table 7). In the cool temperate climate of Haast/Awarua event flow mobilises a significant portion of the dissolved material, on average, 847 t day^{-1} equivalent to 70 % of the dissolved flux (Table 7). This is much higher than chemical weathering fluxes under event flow as observed in the small headwater catchment on the eastern flank of the Southern Alps (Mager et al., 2018), where event flow only accounted for 33 % of the dissolved load flux. The difference is attributed to the frequency of event flow; the Haast/Awarua being on the stoss of the range front in the westerly belt produces conditions of frequent event flow, with flows greater than median occurring, on average 54 % of the year (equivalent to 197 days per year for the period 1970–2021). Significant flow event of a magnitude greater than three times the median flow ($FRE3$) occur >20 times a year. In such circumstances, sampling strategies that focus on limited data collection, or do not consider how the products of chemical weathering rate with hydrographic event flow may be subject to high uncertainties in the flux of dissolved material through river networks. Such observations of the high correlation between chemical weathering flux and runoff (as a surrogate for mean annual rainfall) are commonly reported in other studies (e.g., Kump et al., 2000; West et al., 2002; France-Lanord et al., 2003), but linking the flux of material to event flow also suggests that any changes associated with global climate in the future that may increase storminess, and runoff, may equally influence the amount of material transmitted from denuding landscapes (Beaulieu et al., 2012).

Furthermore, the Haast/Awarua has ample supply of material for

Table 7

Mean dissolved solids yield for the Haast/Awarua derived from hourly-rated discharge records for 2000–2021 and partitioned into base flow and event flow fluxes.

Year	DSY ($\text{t km}^{-2} \text{ a}^{-1}$)	Base flow mean TDS* (t day^{-1})	Event flow mean TDS* (t day^{-1})	Days per year as event flow	Mean TDS _f * (t day^{-1})	Event flux to annual total TDS _f *
2000	225.8	391	893	53 %	657	72 %
2001	199.2	358	837	46 %	580	67 %
2002	214.5	384	848	52 %	624	70 %
2003	201.7	375	784	52 %	587	69 %
2004	230.1	378	848	62 %	670	79 %
2005	188.0	376	753	45 %	547	63 %
2006	203.7	360	846	48 %	593	68 %
2007	191.6	347	816	45 %	558	66 %
2008	202.2	350	869	46 %	588	68 %
2009	216.0	365	909	48 %	628	70 %
2010	220.5	355	936	49 %	642	72 %
2011	207.6	374	834	50 %	604	69 %
2012	188.1	359	801	43 %	547	62 %
2013	219.8	364	908	51 %	640	72 %
2014	222.5	373	855	57 %	647	75 %
2015	222.7	417	827	56 %	648	72 %
2016	229.6	403	850	59 %	668	75 %
2017	185.8	373	765	43 %	541	60 %
2018	203.3	402	772	51 %	592	67 %
2019	251.9	396	979	58 %	733	77 %
2020	228.1	392	877	56 %	664	74 %
2021	230.4	410	806	66 %	671	79 %
Average	211.2	375	847	51 %	615	70 %

mobilisation, so is unlikely to become supply-limited with its wide alluvial channels (e.g., Fig. 2), and steep tributary headwater catchments vulnerable to frequent landslips during storms (Benn, 2005). The largest contributor of suspended material to the Haast/Awarua catchment is from the Landsborough tributary. The confluence between the eponymous Haast tributary and the Landsborough tributary at Clarkes Bluff marks a doubling in flow volume and often a visible increase in turbidity, as well as an increase in specific electrical conductance. The precise factors that contribute to the different hydrochemistry and sediment flux between the two main tributaries are outside the scope of this study and warrant further investigation, but it is suggested that differences in erodibility of the underlying lithology (schist cf. semi-schist), snow and ice coverage (e.g., 43.5 km^2 in the Landsborough,

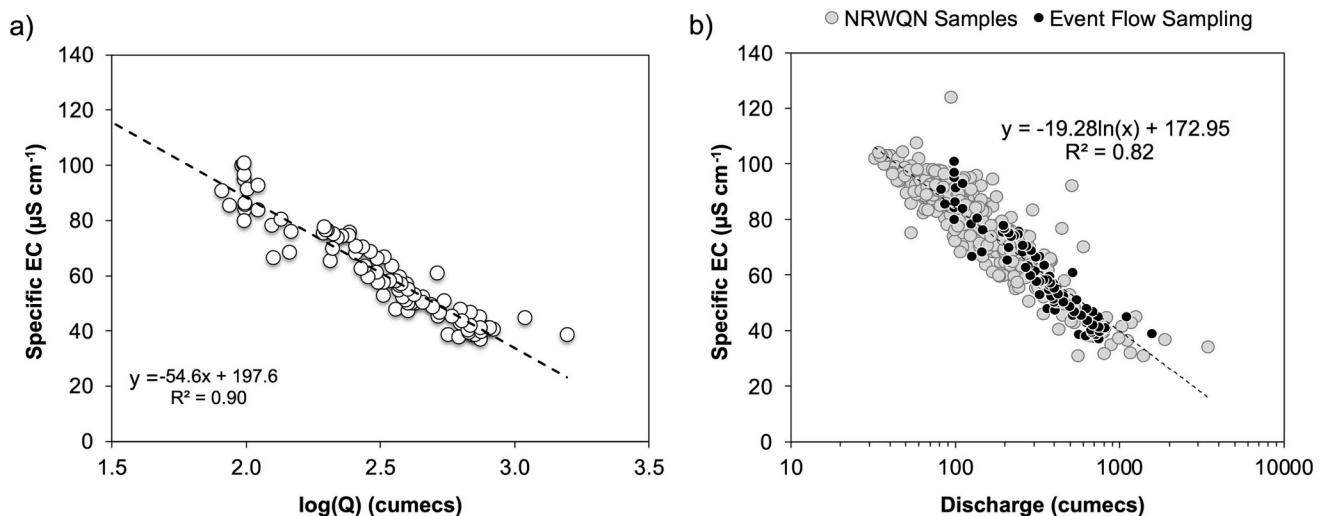


Fig. 5. a) Log-normal plot of event flow rating of discharge ($\text{m}^3 \text{ s}^{-1}$) and observed Specific EC ($\mu\text{S cm}^{-1}$) from hourly water samples collected in the Haast/Awarua for the events 19-Jan-2019, 18-Feb-2019, and 11-Jan-2020 ($n = 100$). b) Specific electrical conductance at the Haast/Awarua River is strongly inversely related to discharge for samples collected under baseflow (1989–2021) so that discharge can be used to predict EC under variable flow conditions.

compared to 4.3 km^2 in the Upper Haast) (e.g., [Beylich and Laute, 2012b](#)), and stores of paraglacial sediment are likely key differences between the tributaries ([Anderson, 2005](#)).

3.4. Reconstructing dissolved load flux from flow records

A continuous time series of total dissolved solids was reconstructed using Specific EC from the NRWQ dataset (and its surrogate TDS*) and rated relative to instantaneous discharge (Q_t) (at the time of sample collection). There was a strong log-normal relationship between dissolved load and streamflow, where Specific EC = $-19.28 \ln Q_t + 172.95$ ([Fig. 5b](#)). Specific EC reaches a minima $\approx 16 \mu\text{S cm}^{-1}$ but thereafter increases in flow do not lead to any further dilution and the rating relationship reaches an asymptote. The rating curve was validated against samples collected hourly over three discrete storm events ([Fig. 5a](#)) and shows that the log-normal rating curve is also a good predictor of TDS* during high flows. The relationship between discharge and Specific EC (and its surrogate TDS*) means that the flow record can be used to reconstruct the dissolved load from 1971 to 2021.

Based on the 51-year daily flow record the mean dissolved flux in the Haast/Awarua is 635 t day^{-1} ([Fig. 6](#)) with daily values ranging from 151 to 2993 t day^{-1} . The mass of material exhumed from the landscape and transported through the river network as an annual specific yield is $218 \text{ t km}^{-2} \text{ a}^{-1}$. There is some interannual variability in the yields, which are due to changes in annual flow. The Interdecadal Pacific Oscillation (IPO) is one of the long-term oscillations that affects the climate of Aotearoa New Zealand, and the strength and frequency of Southern Oscillation (ENSO) events ([Thompson, 2006](#)). Positive IPO values are associated to stronger westerly flows, which result in higher rainfall and runoff generation for the Haast/Awarua. During positive phases of the IPO, the west and south of Southern New Zealand have been shown to be wetter by 8 % ([Salinger et al., 2001](#)). The effect of this change in rainfall can be seen in the small shifts in the dissolved solids yield for the Haast/Awarua, with the estimates of dissolved solids yield (DSY) being moderately correlated to the IPO Index (Pearson's $r = 0.43$ $p < 0.03$).

From this study in near-pristine catchment conditions, ratings of Specific EC and discharge provide a realistic estimate of dissolved load yields relative to discrete monthly sampling estimates (e.g., $209 \text{ t km}^{-2} \text{ a}^{-1}$ in [Table 6](#)) and compare well to estimates previously reported by [Lyons et al. \(2005\)](#). The approach of using flow records also provides a measure of variance of the yield due to variations in flow conditions, and/or longer-term cycles in climate. The proportion of hillslope mass moved in dissolution within the Haast/Awarua represents a small but

often overlooked component of hillslope material transport. The mean annual dissolved flux of $218 \text{ t km}^{-2} \text{ a}^{-1}$ is at the higher end of global estimates of dissolved flux as reported by [Gaillardet et al. \(1999\)](#), exceeding that of the Irrawaddy ($125 \text{ t km}^{-2} \text{ a}^{-1}$) and Purari ($189 \text{ t km}^{-2} \text{ a}^{-1}$) rivers, but not as high as the small headwater Kikori catchment in Papua New Guinea ($338 \text{ t km}^{-2} \text{ a}^{-1}$). Similar rates of dissolved load flux were reported by [Donnini et al. \(2016\)](#) draining the European Alps, where yields average $83 \text{ t km}^{-2} \text{ a}^{-1}$ but ranged from 8 to $411 \text{ t km}^{-2} \text{ a}^{-1}$, with yields $> 200 \text{ t km}^{-2} \text{ a}^{-1}$ restricted to the headwaters of the Lech, Isere, and Isonzo rivers. It is the combination of high mean annual rainfall, frequent slope failure and rapid tectonic uplift rates underpin the processes that yield a dissolved flux in the Haast/Awarua that is a magnitude of order greater than the global average of $24 \text{ t km}^{-2} \text{ a}^{-1}$ ([Gaillardet et al., 1999](#)).

The dissolved flux of $218 \text{ t km}^{-2} \text{ a}^{-1}$ is sustained by carbonate-weathering despite the underlying lithology being dominated by silicates. In the Southern Alps the rapid flushing of material through regular and frequent rainfall events preferentially transports silicates as particulate load and the flux of dissolved material is constrained by the slower chemical reaction times and solubility of silicates relative to carbonate-bearing minerals. This suggests that the underlying lithology of the Southern Alps is chemically less reactive than other terranes and that this caps the potential dissolved load flux in spite of the globally high uplift and rainfall rates. Further work is required that examines in more detail how differences in dissolved load occur along the Southern Alps, and whether specific morphological units are more prone to denudation via chemical weathering processes, as observed in cool nival-dominated catchments by [Beylich and Laute \(2012b\)](#). Additionally, greater emphasis is needed in understanding how estimates of chemical weathering may be influenced by broader changes in climatic conditions, particularly those that affect rainfall distribution in response to larger-scale oscillations.

4. Conclusions

The objective of this study was to reconstruct a multi-decadal flux that considers the effects of seasonal and multi-year variations in hydrochemistry. The flux of dissolved load through the Haast/Awarua River in the southwestern Southern Alps/Ka Tiritiri o te Moana of Aotearoa New Zealand was equivalent to 634 t day^{-1} , of which 70 % of the material was transported during significant storm events. The yield of ionic material exhumed from the catchment was $218 \pm 48 \text{ t km}^{-2} \text{ a}^{-1}$ derived from a 51-year flow record, which is high by global standards,

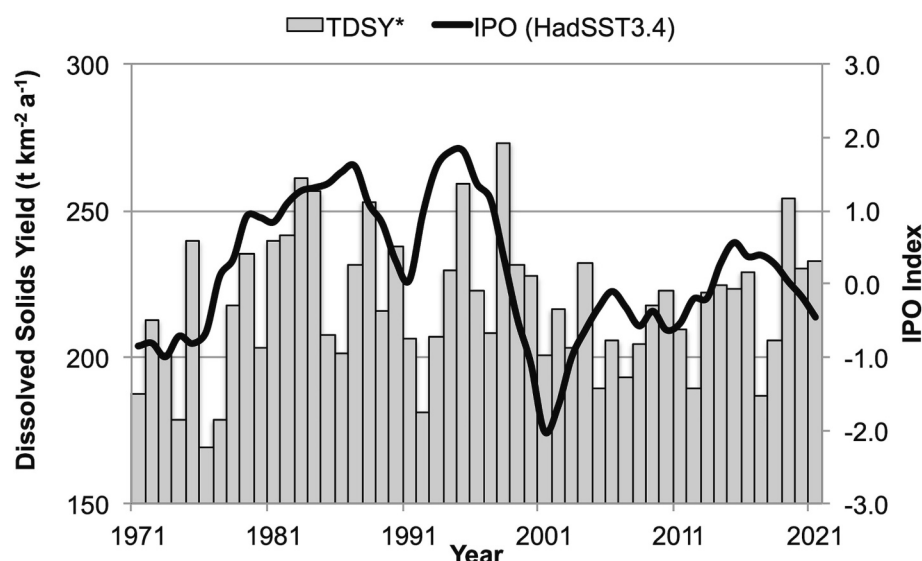


Fig. 6. Annual dissolved solids yield for the Haast/Awarua catchment and the Interdecadal Pacific Oscillation index for each corresponding calendar year.

but falls within the range of 140–442 t km⁻² a⁻¹ derived from previous estimates by Lyons et al. (2005) for the western flank of the Southern Alps. The dissolved yield of the Haast/Awarua has been constructed by developing rating relationships between in-field measurements of Specific EC, measurements of total dissolved solids, and discharge, so that when the bespoke relationships between these variables are known a record of the dissolved load can be reconstructed from discharge records. The underlying assumptions for this rating depend on 1) the catchment having no significant changes in land use or anthropogenic disturbance that may otherwise affect the hydrochemistry, 2) that there exists simple regression relationships between discharge and ionic concentrations, and 3) that under event-flows there are no hysteretic responses in Specific EC.

Funding

This research did not receive any specific grant from funding agencies in the public, commercial, or not-for-profit sectors.

Declaration of competing interest

The authors declare that they have no known competing financial interests or personal relationships that could have appeared to influence the work reported in this paper.

Data availability

NIWA Taihoro Nukurangi National River Water Quality Network data and hydrometric data is available through the online repository: <https://hydrowebportal.niwa.co.nz/>.

Acknowledgements

Flow and water quality data were supplied by NIWA Taihoro Nukurangi. The authors gratefully acknowledge the volunteers who assisted with field sample collection: Christina Bright, Emily Diack, Alex King and Annemaree Senior. Laboratory analysis was supported by Gemma Kerr, Adam Martin, Robert van Hale and Julie Clark at the University of Otago.

References

- Anderson, S.P., 2005. Glaciers show direct linkage between erosion rate and chemical weathering fluxes. *Geomorphology* 67 (1/2), 147–157.
- Anderson, S.P., Drever, J.I., Humphrey, N.F., 1997. Chemical weathering in glacial environments. *Geology* 25 (5), 399–402.
- Asselman, N., 1999. Suspended sediment dynamics in a large drainage basin: the River Rhine. *Hydrol. Process.* 13 (10), 1437–1450.
- Beaulieu, E., Goddérès, Y., Donnadieu, Y., Labat, D., Roelandt, C., 2012. High sensitivity of the continental-weathering carbon dioxide sink to future climate change. *Nat. Clim. Chang.* <https://doi.org/10.1038/NCLIMATE1419>.
- Benn, J.L., 2005. Landslide events on the West Coast, South Island 1867–2002. *N. Z. Geogr.* 63, 3–13.
- Beylich, A.A., Laute, K., 2012a. Seasonal and annual variations of surface water chemistry, solute fluxes and chemical denudation in a steep and glacier-fed mountain catchment in western Norway (Erdalen, Nordfjord). *Catena* 96, 12–27.
- Beylich, A.A., Laute, K., 2012b. Spatial variations of surface water chemistry and chemical denudation in the Erdalen drainage basin, Nordfjord, western Norway. *Geomorphology* 167, 77–90.
- Beylich, A.A., Laute, K., 2018. Morphoclimatic controls of contemporary chemical and mechanical denudation in a boreal-oceanic drainage basin system in central Norway (Homla drainage basin, Trøndelag). *Geogr. Ann. Ser. A Phys. Geogr.* 100 (2), 116–139.
- Blattner, P., Cooper, A.F., 1974. Carbon and oxygen isotopic composition of carbonate dikes and metamorphic country rock of the Haast Schist Terrane, New Zealand. *Contrib. Mineral. Petrol.* 44, 17–27.
- Bouchez, J., Gaillardet, J., 2014. How accurate are rivers as gauges of chemical denudation of the Earth surface. *Geology* 42 (2), 171–174.
- Bright, C.E., Mager, S.M., Horton, S.L., 2020a. Catchment-scale influences on riverine organic matter in southern New Zealand. *Geomorphology* 353, 107010.
- Bright, C.E., Mager, S.M., Horton, S.L., 2020b. Response of nephelometric turbidity to hydrodynamic particle size of fine suspended sediment. *Int. J. Sediment Res.* 35, 444–454.
- Campbell, S.W., Dixon, J.C., Thorn, C.E., Darmody, R.G., 2002. Chemical denudation rates in Kärkevagge, Swedish Lapland. *Geogr. Ann. A* 84 (3/4), 179–185.
- Carey, A.E., Kao, S.-J., Hicks, D.M., Nezat, C.A., Lyons, W.B., 2006. The geochemistry of rivers in tectonically active areas of Taiwan and New Zealand. In: Willett, S.D., Hovius, N., Brandon, M.T., Fisher, D. (Eds.), *Geological Society of America Special Paper 398. Tectonics, Climate, and Landscape Evolution: Geological Society of America Special Paper 398*, Penrose Conference Series, pp. 339–351. [https://doi.org/10.1130/2006.2398\(21\)](https://doi.org/10.1130/2006.2398(21)).
- Cerling, T., Solomon, D.K., Quade, J., Bowman, J.R., 1991. On the isotopic composition of carbon in soil carbon dioxide. *Geochim. Cosmochim. Acta* 55, 3403–3405.
- Cooper, A.F., Paterson, L.A., 2008. Carbonatites from a lamprophyric dyke-swarm, South Westland, New Zealand. *Can. Mineral.* 46, 753–777.
- Dixon, J.C., Thorn, C.E., 2005. Chemical weathering and landscape development in mid-latitude alpine environments. *Geomorphology* 67, 127–145. <https://doi.org/10.1016/j.geomorph.2004.07.009>.
- Donnini, M., Frondini, F., Probst, J.-L., Cardellini, C., Marchesini, I., Guzzetti, F., 2016. Chemical weathering and consumption of atmospheric carbon dioxide in the Alpine region. *Glob. Planet. Chang.* 136, 65–81.
- Duncan, M.J., Woods, R.A., 2013. Water regulation. In: Dymond, J.R. (Ed.), *Ecosystem Services in New Zealand – Conditions and Trends*. Manaaki Whenua Press, Lincoln, New Zealand.
- Emberson, R., Hovius, N., Galy, A., Marc, O., 2016. Chemical weathering in active mountain belts controlled by stochastic bedrock landsliding. *Nat. Geosci. Lett.* <https://doi.org/10.1038/NGEO2600>.
- Finlay, J., 2003. Controls of stream water dissolved inorganic carbon dynamics in a forested watershed. *Biogeochemistry* 62, 231–252.
- France-Lanord, C., Evans, M., Hurtrez, J., Riotte, J., 2003. Annual dissolved fluxes from Central Nepal rivers: budget of chemical erosion in the Himalayas. *Compt. Rendus Geosci.* 335, 1131–1140.
- Gabet, E.J., Wolff-Boenisch, D.W., Langner, H., Burbank, D., Putkonen, J., 2010. Geomorphic and climatic controls on chemical weathering in the High Himalayas of Nepal. *Geomorphology* 122, 205–210. <https://doi.org/10.1016/j.geomorph.2010.06.016>.
- Gaillardet, J., Dupré, B., Louvat, P., Allègre, C.J., 1999. Global silicate weathering and CO₂ consumption rates deduced from the chemistry of large rivers. *Chem. Geol.* 159, 3–30.
- Goldsmith, S.T., Carey, A.E., Lyons, W.B., Hicks, D.M., 2008. Geochemical fluxes and weathering of volcanic terranes on high standing islands: Taranaki and Manawatu-Wanganui regions of New Zealand. *Geochim. Cosmochim. Acta* 72, 2248–2267.
- Goldsmith, S.T., Carey, A.E., Johnson, B.M., Welch, S.A., Lyons, W.B., McDowell, W.H., Pigott, J.S., 2010. Stream geochemistry, chemical weathering and CO₂ consumption potential of andesitic terrains, Dominica, Lesser Antilles. *Geochim. Cosmochim. Acta* 74 (1), 85–103.
- Hicks, D.M., Shankar, U., McKerchar, A.I., Basher, L., Lynn, I., Page, M., Jessen, M., 2011. Suspended sediment yields from New Zealand rivers. *J. Hydrol. (NZ)* 50 (1), 81–142.
- Hilley, G.E., Porder, S., 2008. A framework for predicting global silicate weathering and CO₂ drawdown rates over geologic time-scales. *PNAS* 105, 16855–16859.
- Hren, M.T., Chamberlain, C.P., Hilley, G.E., Blisniuk, P.M., Bookhagen, B., 2007. Major ion chemistry of the Yarlung Tsangpo-Brahmaputra river: chemical weathering, erosion, and CO₂ consumption in the southern Tibetan plateau and eastern syntaxis of the Himalaya. *Geochim. Cosmochim. Acta* 71 (12), 2907–2935.
- Hubert, E., Woldersdorfer, C., 2015. Establishing a conversion factor between electrical conductivity and total dissolved solids in South African mine waters. *Water SA* 41, 490–500.
- Jacobson, A.D., Blum, J.D., 2003. Relationship between mechanical erosion and atmospheric CO₂ consumption in the New Zealand Southern Alps. *Geology* 31, 865–868.
- Jacobson, A.D., Blum, J.D., Chamberlain, C.P., Craw, D., Koons, P.O., 2003. Climatic and tectonic controls on chemical weathering in the New Zealand Southern Alps. *Geochim. Cosmochim. Acta* 67 (1), 29–46.
- Kerr, T., Henderson, R., Sood, A., 2018. The precipitation distribution across Westland Tai Poutini National Park. *J. Hydrol. (NZ)* 57 (1), 1–23.
- Kump, L.R., Brantley, S.L., Arthur, M.A., 2000. Chemical weathering, atmospheric CO₂ and climate. *Annu. Rev. Earth Planet. Sci.* 28, 611–667.
- Larsen, I.J., Montgomer, D.R., Greenberg, H.M., 2014. The contribution of mountains to global denudation. *Geology* 42 (6), 527–530. <https://doi.org/10.1130/G35136.1>.
- Liu, Z., Dreybrodt, W., Liu, H., 2011. Atmospheric CO₂ sink: silicate weathering or carbonate weathering? *Appl. Geochem.* 26, S292–S294.
- Lyons, W.B., Carey, A.E., Hicks, D.M., Nezat, C.A., 2005. Chemical weathering in high-sediment-yielding watersheds, New Zealand. *J. Geophys. Res.* 110, F01008. <https://doi.org/10.1029/2003JF000888>.
- Machado, D.V., Marques, E.D., de Almeida, G.S., Silva-Filho, E.V., 2021. Contribution of the chemical weathering to the CO₂ consumption in a microbasin of Quadrilátero Ferrífero, Brazil. *Environ. Earth Sci.* 80 (17), 1–15.
- Mager, S.M., Diack, E.E., Horton, S.L., 2018. Catchment-scale weathering fluxes in the Southern Alps, New Zealand. *Geomorphology* 316, 24–34. <https://doi.org/10.1016/j.geomorph.2018.05.011>.
- Milliman, J.D., Farnsworth, K.L., 2013. *River Discharge to the Coastal Ocean: A Global Synthesis*. Cambridge University Press.
- Milliman, J.D., Syvitski, J.P.M., 1992. Geomorphic/tectonic control of sediment discharge to the ocean: the importance of small mountainous rivers. *J. Geol.* 100, 525–544.
- Millot, R., Gaillardet, J., Dupré, B., Allegre, C.J., 2002. The global control of silicate weathering rates and the coupling of with physical erosion: new insights from rivers of the Canadian Shield. *Earth Planet. Sci. Lett.* 196, 83–98.

- Mook, W.G., 2006. Introduction to Isotope Hydrology. Taylor and Francis, London, England.
- Moore, J., Jacobson, A.D., Holmden, C., Craw, D., 2013. Tracking the relationship between mountain uplift, silicate weathering and long-term CO₂ consumption with Ca isotopes: Southern Alps, New Zealand. *Chem. Geol.* 341, 110–127.
- Nisha, B.K., Balakrishna, K., Udayashankar, H.N., Manjunatha, B.R., 2021. Chemical weathering and carbon dioxide consumption in a small tropical river catchment, southwestern India. *Aquat. Geochem.* 27 (3), 173–206.
- NIWA Taihoro Nukurangi, 2019. NIWA Hydro Web Portal. <https://hydrowebportal.niwa.co.nz/>.
- Oliva, P., Viers, J., Dupre, B., 2003. Chemical weathering in granitic environments. *Chem. Geol.* 202, 225–256.
- Phillips, D.L., Gregg, J.W., 2001. Uncertainty in source partitioning using stable isotopes. *Oecologia* 127 (2), 171–179.
- Piqué, G., Batalla, R.J., López, R., Sabter, S., 2017. The fluvial sediment budget of a dammed river (Upper Muga, Southern Pyrenees). *Geomorphology* 293, 211–226. <https://doi.org/10.1016/j.geomorph.2017.05.018>.
- Pope, G.A., Dorn, R.I., Dixon, J.C., 1995. A new conceptual model for understanding geographical variations in weathering. *Ann. Assoc. Am. Geogr.* 85, 38–64.
- Rattenbury, M.S., Jongens, R., Cox, S.C., 2010. Geology of the Haast area. Institute of Geological & Nuclear Sciences 1:250 000 Geological Map 14. GNS Science, Lower Hutt, New Zealand (compilers, 1 sheet + 58 p.).
- Riebe, C.S., Kirchner, J.W., Granger, D.E., Finkel, R.C., 2001. Strong tectonic and weak climatic control of long-term chemical weathering rates. *Geology* 29 (6), 511–514.
- Roser, B., Cooper, A., 1990. Geochemistry and terrane affiliation of Haast Schist from the western Southern Alps, New Zealand. *N. Z. J. Geol. Geophys.* 33 (1), 1–10. <https://doi.org/10.1080/00288306.1990.10427567>.
- Rounick, J.S., Winterbourn, M.J., Lyon, G., 1982. Differential utilization of allochthonous and autochthonous inputs by aquatic invertebrates in some New Zealand streams: a stable isotope study. *Oikos* 39 (2), 191–198.
- Salinger, M.J., Renwick, J.A., Mullan, A.B., 2001. Interdecadal Pacific Oscillation and South Pacific climate. *Int. J. Climatol.* 21, 1705–1721.
- Stewart, D.P.C., Metherell, A.K., 1999. Carbon (¹³C) uptake and allocation in pasture plants following field pulse-labelling. *Plant Soil* 210, 61–73.
- Tait, A., Henderson, R., Turner, R., Zheng, X., 2006. Thin plate smoothing spline interpolation of daily rainfall for New Zealand using a climatological rainfall surface. *Int. J. Climatol.* 26 (14), 2097–2115. <https://doi.org/10.1002/joc.1350>.
- Thompson, C.S., 2006. Relative influence of the Interdecadal Pacific Oscillation on drought occurrence and severity. *Weather Clim.* 26, 35–66.
- Vercruyse, K., Grabowski, R., Rickson, R., 2017. Suspended sediment transport dynamics in rivers: multi-scale drivers of temporal variation. *Earth-Sci. Rev.* 166, 38–52.
- West, A.J., Bickle, M.J., Collins, R., Brasington, J., 2002. Small-catchment perspective on Himalayan weathering fluxes. *Geology* 30 (4), 355–358.